Is the Gas-Fed PPT an Electromagnetic Accelerator? An Investigation using Measured Performance *

J.K. Ziemer† and E.Y. Choueiri‡
Electric Propulsion and Plasma Dynamics Laboratory (EPPDyL)
Mechanical and Aerospace Engineering Department
Princeton University, Princeton, New Jersey 08544

Daniel Birx
Science Research Laboratory Inc.
Sommerville, MA 02143

AIAA-99-2289§

Abstract

We present a new gas-fed pulsed plasma thruster performance database and use it to investigate the electromagnetic nature of the acceleration process by identifying trends in the dependencies of the performance parameters on the mass bit, energy, and capacitance. It was previously observed[1] that performance measurements for PPTs operating at low mass bits (< 2 μg per pulse) can be influenced by contamination from diffusion pump oil. Consequently, facility renovations and a new impulse measurement protocol using liquid nitrogen cooled baffles to reduce diffusion pump oil backstreaming were implemented and are discussed. A portion of the database has been duplicated in a cryo-pumped facility at NASA-JPL to verify that the contamination effects have been removed. The intermittent simultaneous operation of the discharge initiation plugs, that was previously observed to degrade the performance, was solved with a new electric circuit and the resulting discharge symmetry verified using a fast-framing camera. The nature of the acceleration process is examined by comparing trends in the performance database with the theoretically expected scaling for electromagnetic acceleration. The performance was found to transition with decreasing mass bit (or increasing I_{sp}) from a mode (Mode I) where the efficiency and the impulse are respectively independent and dependent on the mass bit (and where the efficiency the thrust to power ratio are respectively independent and dependent on I_{sp}) to another mode (Mode II) where the converse statements hold. Furthermore, in mode II the efficiency is independent of energy level and both the efficiency and the thrust-to-power ratio scale with the square root of capacitance as expected in a predominantly *electromagnetic* accelerator.

1 Introduction

The question of whether the dominant acceleration mechanism in pulsed plasma thrusters (PPTs) is electromagnetic or electrothermal is of current interest[2, 3] and is important not only due to its fundamental value but also due to its implications on improving propulsive performance and clarifying how to properly scale these devices to higher or lower discharge energies.

The goal of this study is twofold: 1) present a performance database measured with a modern GFPPT operating over a wide range of mass bits, energy levels, and driving capacitance values and 2) use the measured performance trends to investigate the question about the nature of the acceleration. The goal is *not* to present the best performance data that can

*Research supported by the Air Force Office of Scientific Research, grant number: F49620-95-1-0291, NASA JPL Advanced Propulsion Group, and the Plasma Science and Technology Program at the Princeton Plasma Physics Lab.

†Graduate Student, Research Assistant. Member AIAA.

‡Chief Scientist at EPPDyL. Assistant Professor, Applied Physics Group. Senior Member AIAA.

§Presented at the 35^{th} AIAA Joint Propulsion Conference, Los Angeles, CA, June 20-23, 1999.

be attained with a given thruster.

Although the dominant acceleration mechanism of ablative pulsed plasma thrusters (APPTs) may still be under debate, trends in this database as discussed in this paper indicate that for a typical *gas-fed* PPT, the performance can be easily be made to transition to a mode where the trends follow the expected scaling of electromagnetic acceleration.

Previous performance measurements at EPPDyL[4, 5] as well as Fairchild Republic[6] in 1966 have been shown to be influenced by diffusion pump oil contamination. A thin oil-film is believed to build up on the thruster electrodes between impulse measurements and influence the discharge dynamics due to the small mass bit nature ($< 2\mu$g per pulse) of GFPPT operation. Steps have been taken at EPPDyL to eliminate this problem including modifying existing baffles to accept liquid nitrogen cooling and develop a protocol for thruster decontamination and conditioning.

This paper begins by describing the current GFPPT system (PT5) studied in this database and improvements to the discharge initiation circuitry to insure a reliable, symmetric, and simultaneous breakdown at the start of the GFPPT discharge. The next section describes the issue of diffusion pump oil contamination, a comparison of the performance measurements taken at EPPDyL's recently renovated facility with impulse measurements taken at a cryo-pumped facility at NASA JPL, and an outline of a new procedure for eliminating contamination effects from performance measurements. The performance measurement technique used for this database is detailed along with an error analysis of measured parameters. Finally, The results of the database are presented with a discussion of trends and a comparison of the data set to a simple electromagnetic acceleration model.

2 The PT5 GFPPT

A detailed description of the SRL family of GFPPTs has been given in other papers[4, 5, 7] and will only be summarized here. A steady-state power supply charges the PPT capacitor bank which is discharged at a finite duty cycle between two co-axial electrodes where gas has been injected just before the pulse (see Fig. 2). If the gas discharge initiation is uniform, a disk-like current sheet forms and is accelerated due to the Lorentz force created by the current flowing through the sheet and the self-induced magnetic field. The plasma current sheet acts like a piston or snowplow on the gas in front of it and exhausts the gas at a velocity of a few tens of km/s. Typical operational parameters for one pulse include charging voltages close to 250 V, peak discharge currents on the order of 10 kA, and discharge durations of less than 10 μs. During the pulse, instantaneous power is close to a megawatt, however, the duration is short enough that only 1-10 J of stored energy is necessary for each pulse.

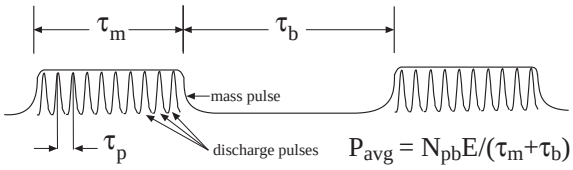

Figure 1: Schematic of a burst of pulses.

Until recently GFPPTs suffered from low propellant utilization efficiency due to the fact that the fastest available space-qualified gas valve with long enough life ($> 10^7$ pulses) has an open time not shorter than 1 ms. As the time to fill the discharge chamber is only the on the order of 100 μs, much of the propellant could not utilized effectively over the life of the device. Recent work has resulted in a complete solution[4] to this problem by using state-of-the-art pulse power technology raising the propellant utilization efficiency to well above 90%. This solution is illustrated in Fig. 1 and relies on using modern pulsed-power conditioning technology to adjust the period τ_p between pulses to a length very close to the time it takes for the cold injected gas to fill the thruster chamber. This typically corresponds to pulse frequencies of a few kHz during the burst. Depending on the available bus power and mission requirements, sets of such pulses can be produced such that each lasts a period τ_p that is at least as long as the response of a space-qualified valve (e.g. 1 ms) thus making sure that practically all injected propellant is utilized. A typical voltage and mass flow rate history of multiple pulses is shown in Fig. 1.

The fifth-generation SRL-GFPPT used in the present study is designated as PT5 and has undergone five additional modifications since its original design including changes to its discharge initiation system and propellant distribution[7]. A schematic of PT5 is shown in Fig. 2. The PT5 has a relatively large, stainless-steel co-axial set of electrodes with an outer to inner electrode radius ratio of approximately

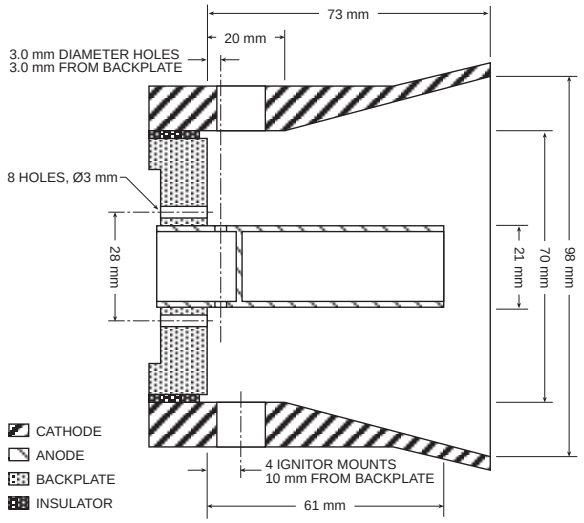

Figure 2: Schematic of PPT5.

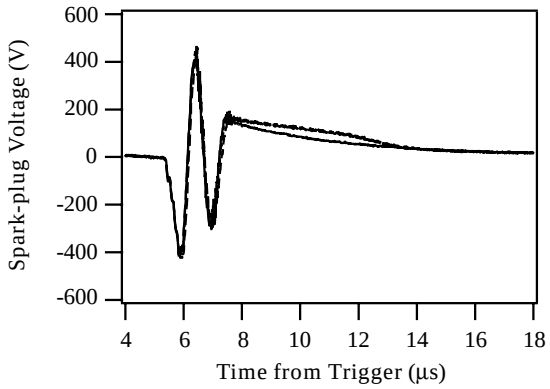

Figure 3: Voltage on all four spark plugs during discharge.

four and a total volume of 350 cm^3. It uses four semi-conductor type spark plugs mounted on the inside of the outer electrode (cathode) at 90 degree azimuthal intervals to initiate the discharge uniformly. The main discharge is driven by a low-inductance ($<$ 10 nH) 130 or 270 μF capacitor bank which is capable of being charged to 250 V giving a maximum energy per pulse of 4 or 8 J, respectively. The entire thruster has a mass of approximately 6 or 8 kg depending on the capacitance level and including the electrode mass as well as the thruster housing mass. The latest modification involves a new discharge initiation circuit that provides reliable, simultaneous activation of all four spark plugs at the beginning of the discharge as described in the next section.

2.1 New Parallel Discharge Initiation Circuit

The design of the discharge initiation (DI) system for co-axial geometry GFPPTs has undergone many revisions at EPPDyL to improve repeatablity, spark plug lifetime, and discharge symmetry. In the last iteration, the same Bendix semi-conductor type spark plugs used in the LES8/9 ablative pulsed plasma thruster (APPT) were adopted for their low breakdown voltage characteristics [8] and demonstrated long-lifetime. Firing four or more spark plugs *simultaneously* to create a uniform and symmetric discharge, however, was found not to be a trivial task. Discharge asymmetry due to one or more spark plugs not firing at all was shown by fast-framing camera images of co-axial GFPPT discharges over many different operating conditions [7]. In addition, as described in Section 3.3, performance measurements conducted at NASA JPL showed that the impulse bit was reduced by as much as 40% when only one spark plug fired instead of four.

To correct this problem, the spark plugs were removed from the outer electrode of the PT5 and an entirely new discharge initiation system was designed and tested in a small high-vacuum facility which allowed for quick modifications. First, the ignition characteristics of one spark plug were tested over a wide range of background argon pressures (0.1-10 millitorr) and applied voltages (200-1000 V) using a 0.2 μF capacitor on the primary side of a 10x pulse transformer. The breakdown condition of this type of spark plug was found to be a strong function of the time derivative of the voltage, the absolute magnitude of the applied voltage, and the internal resistance of the spark plug. Breakdown was found to be a weak function of argon pressure although the argon in these tests was supplied as a background gas and did not directly impinge on the spark plugs as it does in the PT5 configuration. Minimal breakdown conditions for a typical spark plug at 1 millitorr of argon were found to include a $\mathrm{dV/dt} > 400V/\mu s$ and an absolute voltage greater than 250 V as shown in a sample voltage trace of four spark plugs in Fig. 3.

As the spark plug testing continued, the internal resistance of each spark plug changed over a wide range of values between 200 and 2000 Ω generally increasing with the number of pulses fired although

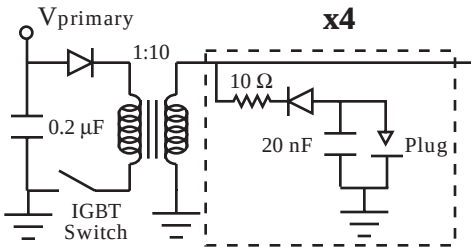

Figure 4: Schematic of the new discharge initiation circuit. The portion of the circuit surrounded by the dashed box is repeated four times in parallel, one for each spark-plug.

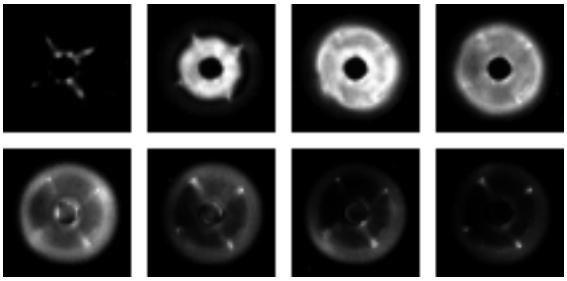

Figure 5: Imacon Fast-Framing Camera photos of a typical PT5 discharge looking head on into the discharge chamber at 0.5 μg per pulse at 4 J of energy. The photos seen here are spaced by 1 μs going from right to left.

not monotonically. The breakdown voltage characteristics increased with increasing internal resistance leading to a slightly higher requirement for the dV/dt and absolute voltage magnitude in order for all the spark plugs to break down regardless of internal resistance. Once this was determined, a DI circuit that could produce the necessary voltage characteristics to all four spark plugs connected in parallel (common cathode) was designed and tested.

Following a similar design to the Fairchild DI circuit in the LES8/9 APPT, the secondary side of the original pulse transformer was modified to include a high-voltage, 20 nF mylar capacitor in parallel with the spark plug. In addition, a high-current, fast-switching diode (International Rectifier part HFA15TB60) and 10 Ω resistor in series with the spark plug were used to insure that each capacitor did not lose its charge to another spark plug already in the process of breaking down. This is important as the first spark plug to fire provides the lowest impedance path that can drain the other spark plugs' capacitors before they have had the chance to fire. A schematic of the new DI circuit is shown in Fig. 4.

2.2 Discharge Initiation Symmetry

The new DI circuitry was installed on PT5 and the thruster was tested under a variety of operating conditions including changes to the DI primary capacitor voltage. The DI circuit was found to operate most effectively and repeatably with a primary capacitor voltage of 500 V. Although initiation at higher voltages worked equally well, the primary capacitor voltage was kept at a minimum to reduce the energy added to the discharge by the spark plugs and to reduce the possible erosion of the spark plug material due to higher current operation. Impulse was measured as a function of primary capacitor voltage and did not noticeably change until the primary voltage exceeded 800 V, however, even then only slightly, <5%. At a primary capacitor voltage of 500 V, only 25 mJ of energy are necessary for the discharge initiation including all four spark plugs.

High-speed photographs of the discharge were taken with an Imacon Fast-Framing Camera (IFFT) at rates of 500,000 frames per second. This diagnostic tool has been used before [7] to examine the symmetry of the discharge with an exposure to all visible wavelengths of light and was used in a similar fashion here. A series of IFFT frames of PT5 with the new DI circuitry are shown in Fig. 5 and show the resulting discharge symmetry.

3 Contamination Reduction at EPPDyL

Unlike previous pulsed thrust measurements at EPPDyL where impulse bits > 280 μNs[1] were measured repeatably, lower impulse bit measurements have shown signs of magnitude decay that seem to implicate pump-oil contamination effects. In these performance measurement experiments consisting of multiple repetitive trials with small mass bits, the magnitude of the impulse bit has been seen to decrease as the total number of pulses increases as can be seen in Fig. 6. This impulse bit decay was first

[1]This number corresponds to the impulse bit of an LES8/9 APPT measured at EPPDyL[9] that agrees with measurements from other laboratories, for example[10].

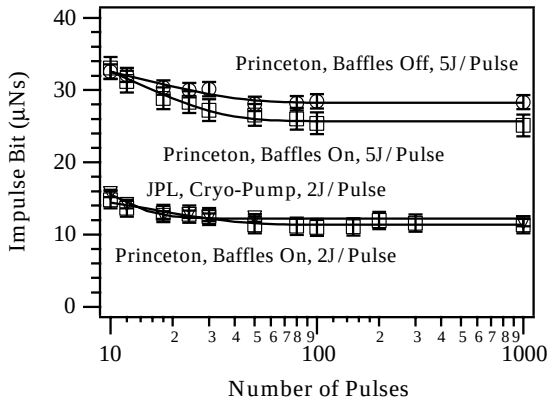

Figure 6: Impulse bit decay as a function of the number of pulses at two different energies and two different facilities.

noted in experiments in Princeton last summer[1] and has also been noticed before in other experiments with GFPPTs where changing surface conditions were blamed[6]. To a large extent the accumulation of diffusion pump oil (used at Princeton for obtaining high vacuum) on the electrodes of the thruster has been blamed for the initially high impulse values. Line emission spectroscopy indicated that as more pulses are fired, more of the oil is removed from the electrodes gradually reducing the amount of extra mass and extra impulse provided by the contaminant to the discharge. As the number of pulses increases, the impulse value seems to reach an asymptote providing a "clean" data point.

Consequently, a substantial effort has been invested in cleaning the vacuum facility and modifying the existing baffle system to accept liquid nitrogen and reduce backstreaming as much as possible. These activities are described in detail in the appendix.

3.1 Overall Diffusion Pump Oil Contamination Reduction

To measure the level of background oil vapor, a UTI 100C residual gas analyzer (RGA) was connected to the tank through an isolation valve mounted on one of the optical ports at the end of the tank. The isolation valve was kept closed unless the LN_2 baffles were activated to reduce the possibility of the ionizing filament or faraday cup becoming contaminated. In addition, before making any of the measurements presented in this paper, the entire RGA unit was baked at close to 200°C for over 48 hours to remove any contaminants from the gauge walls. Figure 7 shows a typical mass spectrum produced by the RGA just as the baffles were activated and two hours later. This figure also shows the predicted spectra of DC 704 diffusion pump oil and conventional Duo-Seal roughing pump oil both used in the high vacuum facilities at EPPDyL. Many of the peaks shown in Fig. 7 match up with those predictions indicating that diffusion and roughing pump oil vapors exist, however, at very low levels (partial pressures on the order of 20 $\times 10^{-9}$ Torr) compared to the background nitrogen levels. This data also shows an overall trend of about 50% reduction in background gases over a wide range of atomic masses. Choosing one atomic mass over charge value as a representative for diffusion pump oil levels (78 amu/e) and roughing pump levels (57 amu/e) allows a quantitative assessment of background vapor level during baffle cooling. These two levels were chosen from a list of maximum peaks in various cracking patterns. A graph showing the reduction of oil and water vapor as a function of time and baffle temperature is shown in Fig. 8. Again, this shows approximately a 50% reduction of possible contaminants after the baffles have been cooling for over 100 minutes down to a temperature of -60°C. This reduction level was confirmed by opening the RGA isolation valve for a short time after the liquid nitrogen cooling was deactivated and the baffles were allowed to completely warm up. The levels measured by the RGA at that time returned to the previous value before the baffles were activated.

3.2 Discharge Cleaning of SRL5e-GFPPT

Both spectroscopic studies and impulse measurements have shown that performance and background oil levels reach an asymptote after a small number of pulses indicating that the high current GFPPT discharge cleans potential contaminants off the electrodes on every pulse. Occasional breaks between pulses occur while waiting for the thrust arm to naturally relax back to its neutral position and during the cold gas measurements. These breaks between discharges can allow more deposits to build up which must then be cleaned off before accurate impulse measurements can be made. By experimenting with various delays between bursts, impulse bit increases were noticed (>5% increase) repeatably only for breaks larger than 10 minutes. A period of 50 seconds used between all bursts described in this pa-

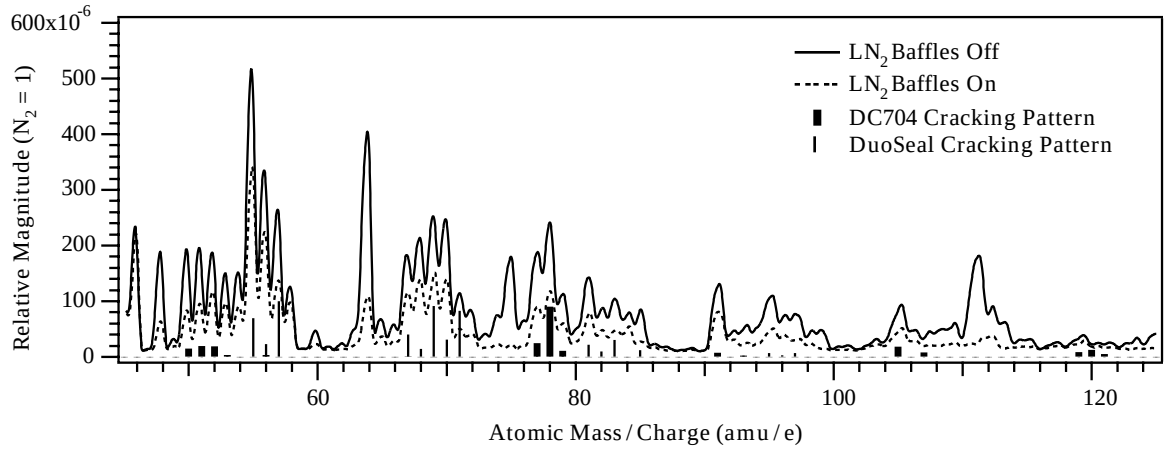

Figure 7: Mass spectrum of background gases from the RGA with baffles on and off as well as expected DC704 diffusion pump oil and DuoSeal roughing pump oil cracking patterns.

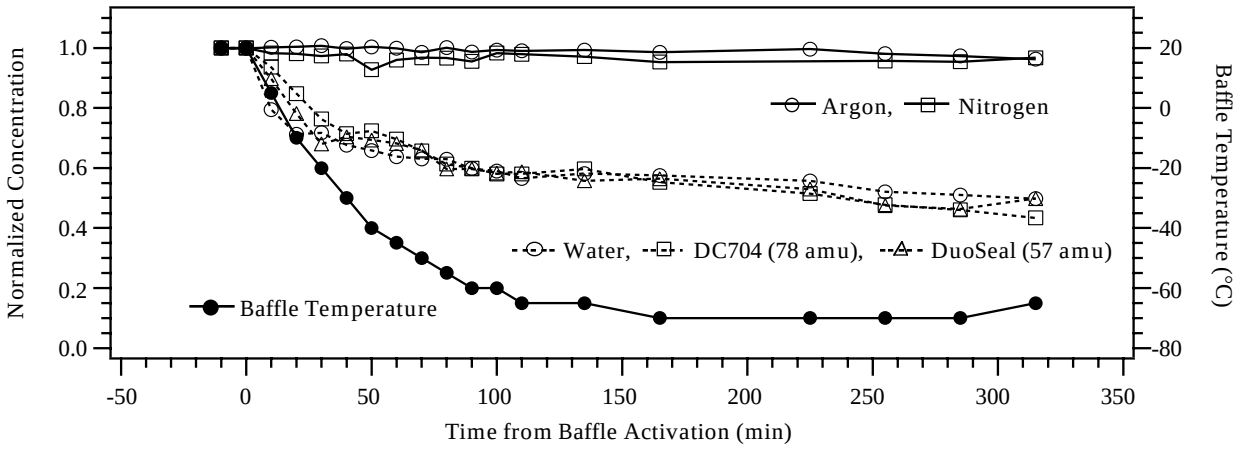

Figure 8: Baffle temperature and background gases as a function of time from baffle activation.

per is considered a short enough time to insure an insignificant amount of oil has been deposited on the electrodes between trials.

RGA data taken after the electrodes had been cleaned by many discharges still showed a tenfold increase in DC 704 oil levels *immediately* after each burst. However, simultaneously, the increase in the argon levels due to the propellant flow were measured to be 1000 times larger than the oil levels. Oil level increases were much larger on the first few bursts after long delay without firing, however, levels returned to their lower steady values after only four or five bursts. From this observation, we can conclude that after the electrodes have been properly cleaned, the amount of oil residue in the discharge is minimal.

Using the discharge as a method for cleaning the thruster is a technique in the new performance measurement protocol at EPPDyL. As seen in Fig. 6, after an extended break, and especially after pump-down, at least 60 pulses (10 bursts) are required to bring the impulse bit level down to the asymptote that agrees with data taken at NASA-JPL immediately after pump-down.

3.3 Comparison of Results with Impulse Measurements at NASA JPL

In order to confirm that the asymptote level apparent after approximately ten bursts of six pulses each is a "clean" data point, the PT5 was tested in a known clean environment (a cryo-pumped facility that is only exposed to roughing pump oil during the pump-down phase of operation) at the same operating conditions.

Performance measurements taken at JPL were conducted in a 1.5 m diameter, 2.0 m long steel tank containing a Princeton-designed thrust stand (see Fig. 9) at NASA JPL. A CVI TM500 twenty inch cryo-pump brings the tank to an operating pressure of 1.5×10^{-6} Torr without propellant flow. Tank pressure peaked below 4×10^{-5} Torr during the maximum pulsed argon propellant flow. Care was taken to minimize mechanical pump oil back-streaming during rough pumping which was suspected to be a cause of contamination that can affect performance measurements. The impulse and performance measurements are made in a similar way to those at EPPDyL as described in Section 4.

Figure 6 shows both data taken at Princeton before the renovations at higher energy per pulse, 5 J, and data taken after the renovations using the same

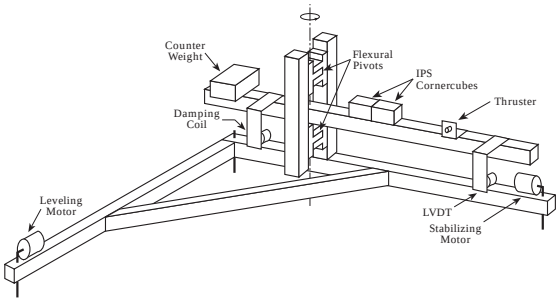

Figure 9: JPL micro-thrust stand.

operating conditions as those tested at NASA JPL, approximately 2 J per pulse and 0.5 μg per pulse. Activation of the baffles reduced the asymptote level by 11% at the higher energy level while providing agreement within the error bars to the data set from JPL. In all cases, at least 50 pulses are required to reach the asymptote.

3.4 Impulse Measurement Protocol

A protocol for performance measurements that are free of contamination effects was developed in light of the above described experiments. It includes the following three guidelines:

1. The LN_2 baffles must be activated for at least 100 minutes before testing to reach the correct impulse asymptote

2. After pump-down or extended times between hot pulses, 1000 pulses should be fired to insure that the thruster electrodes are clean and the impulse magnitude has reached an asymptote level.

3. Because of the ten minute break between hot pulses caused by routine cold gas measurements, the first 10 bursts (60 pulses) of 30 bursts at one operating condition should be ignored to insure uncontaminated impulse measurement.

This protocol was followed for every performance data point reported here.

4 Performance Measurements of PT5

For a GFPPT, performance is calculated based on the impulse produced by a measured amount of stored

energy and the measured amount mass that was accelerated. The efficiency of a PPT is defined here in the conventional manner as a ratio of the directed kinetic energy to the initial stored energy,

$$\eta \equiv \frac{\frac{1}{2}m_{bit}\bar{u}_e^2}{\frac{1}{2}CV_0^2} = \frac{I_{bit}^2}{m_{bit}CV_0^2}, \tag{1}$$

where the mass bit, m_{bit}, is found from the mass flow rate as described in Section 4.2, the average exhaust velocity, $\bar{u}_e$, is defined as $\bar{u}_e \equiv I_{bit}/m_{bit}$, C is the measured capacitance, V_0 is the measured initial voltage on the capacitor, and I_{bit} is the average impulse of one pulse in a burst or the "impulse bit". For a PPT, the thrust-to-power ratio is the same as the impulse bit to energy bit ratio,

$$\frac{T}{P} = \frac{I_{bit}}{E} = \frac{I_{bit}}{\frac{1}{2}CV_0^2}. \tag{2}$$

Finally, the specific impulse is the amount of impulse provided by the thruster per unit weight on earth of the propellant used in the pulse,

$$I_{sp} = \frac{I_{bit}}{m_{bit}g_0} = \frac{\bar{u}_e}{g_0}. \tag{3}$$

To evaluate these parameters, three measurements are required for each individual pulse: stored energy, mass bit, and impulse bit. For all data presented in this paper, a train of six pulses was fired per trial at close to 270 μs intervals. All results consist of what would be the average value of a single pulse in that train. The techniques for finding these average per-pulse values are described below and a schematic of the entire experimental set-up is shown in Fig. 10.

4.1 Pulse Energy Determination

The primary capacitor voltage is measured at the charging supply through a calibrated 1000:1 voltage probe. For each set of pulses, a voltage trace is captured on a digital oscilloscope showing the charging and discharging cycle of the capacitor for all the pulses in the burst. The oscilloscope is set to acquire the discharge voltage history with sufficient speed and resolution to allow the current history to be accurately inferred from the numerical voltage derivative. To determine the energy per pulse, the voltage trace is squared and multiplied by the measured capacitance with a typical accuracy of within 1.5 %. The peak energy before every pulsed is averaged to determine the energy per pulse and the standard deviation of that average is used as the error in this measurement. For most measurements, this error is below 4%.

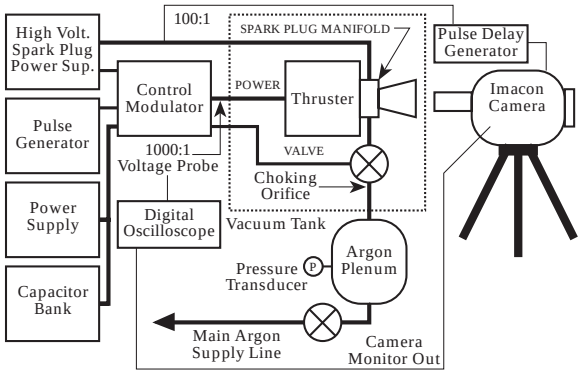

Figure 10: Schematic of the SRL-GFPPT experiment including the Imacon camera and related equipment.

4.2 Mass Bit Determination

Propellant, in this case argon, is supplied to PT5 through a valve, choking orifice, and plenum arrangement as shown in figure 10. The valve is located approximately 10 cm upstream from the thruster propellant injection ports. It is opened and closed by the control module and timed by a signal generator. For these experiments, the valve was open for 45 ms and the thruster was set to fire 40 ms after the valve opened to allow sufficient time for the gas to reach a steady flow rate. This time could be reduced with faster acting valves. The mass flow rate is controlled by changing the pressure in the plenum upstream of the sonic orifice. Soon after the valve is open, the flow is choked and a steady-mass flow rate is reached. In this case, the sonic orifice is a copper plate with a 0.36 mm hole. The mass flow rate as a function of plenum pressure was measured to calibrate the sonic orifice before the database was taken.

The mass bit value itself comes from the timing of the pulses within a burst. This timing is determined from the main capacitor voltage trace. Except for the first two pulses which are slightly longer, all the later pulses have close to 270 μs between discharges. This time multiplied by the mass flow rate generates an average mass bit for each pulse in the pulse train. Obviously, for the first pulse, mass is entering the thrust chamber for much longer than 270 μs, however, the cold gas exhaust velocity has been measured at close to 400 m/s. At that speed, if the gas is moving primarily in the axial direction, it would begin to leave the thrust chamber after only about 200 μs. Therefore, we expect similar gas loading conditions for each pulse.

4.3 Impulse Measurement

The impulse produced by a PPT discharge is measured by monitoring the position of the thruster mounted at the end of a swinging gate type thrust stand. The thrust stand has a vertical rotational axis through two flexural pivots that allows relatively free rotational motion in the horizontal direction. Knowing the position of the thruster at all times allows the impulse to be determined based on calibrated thrust stand dynamics. These dynamics as well as the position measurement system are described in ref. [9].

4.4 Measurement Sequence and Error Analysis

The sequence of experimental trials was designed to reduce the average error in the measurements through repetitive testing at the same conditions. One data point represents the operation of the thruster at one initial stored energy value and one mass bit condition. As described in Section 3.4, one data point is made up of 40 impulse measurement trials including 10 cold-gas pulses (where the thruster capacitors are not charged) and 30 "hot" pulses used to determine the impulse bit and shot-to-shot repeatablity.

In all the trials, the impulse is actually measured for one *burst* of pulses and the impulse bit of a particular trial is the *average* impulse per pulse in the burst obtained by measuring the impulse and dividing by the number of pulses in a burst. Since the propellant flows for much longer than the burst time, typically 65 ms of effective gas flow compared to 2 ms of pulses, during thruster operation the cold-gas contribution to the impulse is completely subtracted before any performance calculations are made. This subtraction yields the hot impulse value. The cold-gas impulse is determined for each mass bit by averaging 10 trials at the same plenum pressure without charging the main capacitors. All the impulse data presented in this report are found by averaging the hot impulse values from the last 20 of the 30 hot trials. The first ten trials at any condition are discarded due to the impulse bit decay phenomena present in the data as discussed in Section 3.

The error in measuring a particular impulse comes from the effective mass calibration error, the error in measuring the thrust arm velocity just before the impulse accurately, and the random noise in the position history. Putting these factors together, the average error for a single impulse measurement is $< 3\%$. Typically the average cold-gas impulse from 10 trials has a standard deviation of $\pm 3\mu$Ns out of a typical value of 100 μ Ns indicating good shot-to-shot repeatablity with a small error. The average hot impulse has a standard deviation of $\pm 10\mu$Ns out of typically 100μNs or about $\pm$ 10%. This deviation is a result of deviations of energy, mass-bit and spark plug operation from pulse to pulse. Performance parameters such as efficiency and the thrust-to-power ratio are calculated from measurements made on individual trials to bring out this correlation and reduce the overall error. The final error associated with each performance parameter is simply the standard deviation of the average parameter value over 20 measurements at the same conditions. Typical errors for the efficiency and thrust-to-power ratio are near 10%.

4.5 Experimental Results

Two energy levels for each of two capacitance values were tested over ten different mass bit values each yielding a 40-point GFPPT performance database. Four graphs which show PT5 performance as a function of mass bit and specific impulse with the capacitance and the initial stored energy level as parameters are shown with error bars in Fig. 11. The lines between the data points are simple fourth order polynomial curve fits meant to show overall trends apparent in the data, however, this is not necessarily the correct functional form to the data. The coefficients for the curve fits are not shown here as the chosen curve-fit function did not always match the data well, especially at low specific impulse values. Tables of the performance data are given at the end of this article.

5 Discussion

It is evident from all the plots in Fig. 11 that there is for each curve a transition with decreasing mass bit (or increasing I_{sp}) from a mode (Mode I) where the efficiency and the impulse are respectively independent and dependent on the mass bit (and where the efficiency the thrust to power ratio are respectively independent and dependent on I_{sp}) to another mode (Mode II) where the converse statements hold.

We now explore these trends and their significance using the theoretically expected scaling corresponding to electromagnetic or electrothermal acceleration.

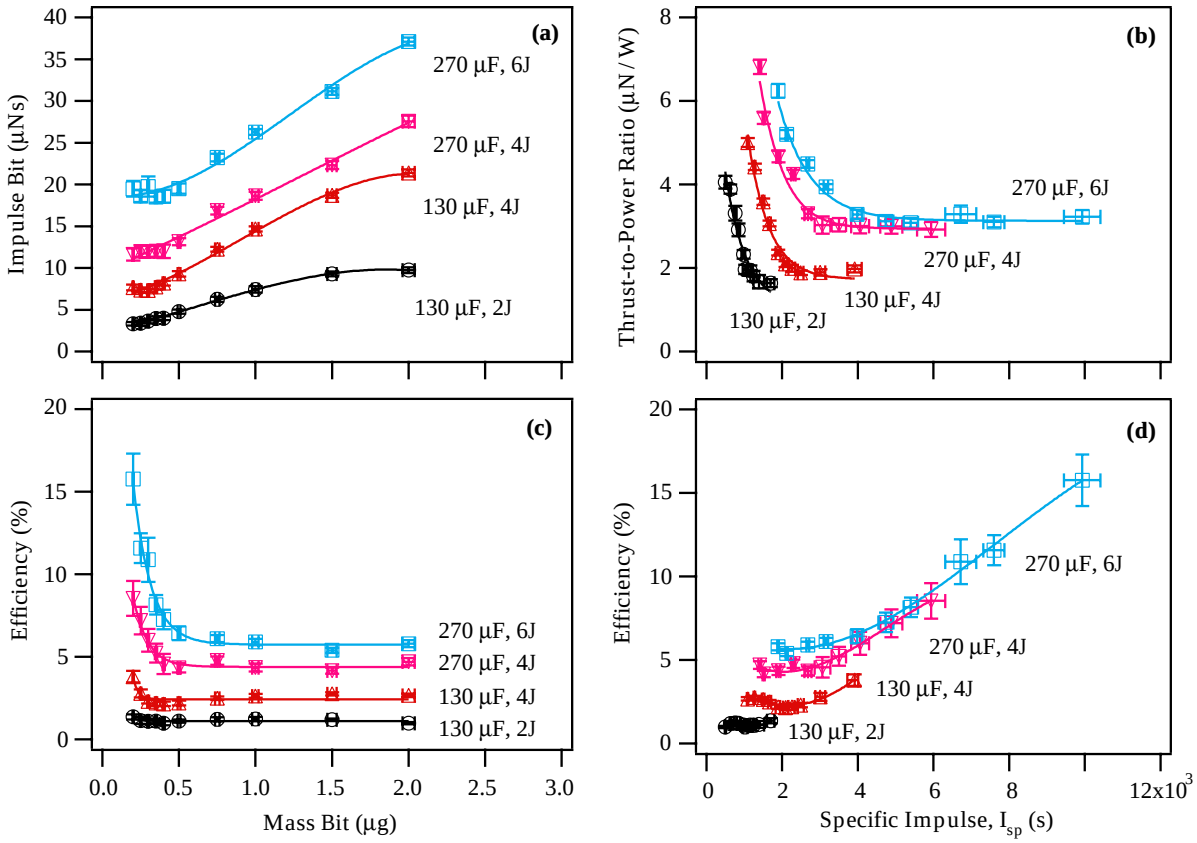

Figure 11: Performance of PT5. Graphs (a) and (c) show the impulse bit and efficiency as a function of mass bit. Graphs (b) and (d) show the thrust-to-power ratio and efficiency as a function of specific impulse. All graphs contain four curves which show changes in performance due to changing capacitance values and initial stored energy levels.

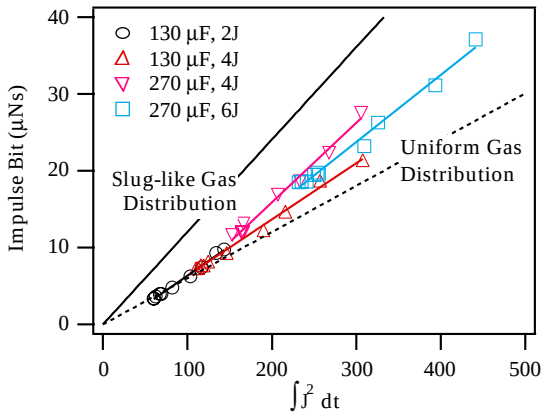

Figure 12: PT5 impulse bit as a function of the integral of the current squared during the discharge. Two lines showing the predicted performance from electromagnetic theory for two different mass distributions are also shown.

5.1 Theoretical Electromagnetic Performance

Simple models neglecting the gas dynamics of sweeping up the mass in front the snow-plow-like current sheet have been presented and used before to examine PPT performance trends [1, 2, 5, 11]. Most of these models assume an equivalent RLC circuit for the discharge including a variable inductance, a fixed capacitance and a resistance based on the plasma conductivity. The simplest relation for the impulse bit of a self-field, co-axial PPT based on an electromagnetic acceleration mechanism is,

$$I_{bit} = \frac{\mu_0}{4\pi} \ln \frac{r_{out}}{r_{in}} \int J^2 dt = \frac{1}{2} L_1 \int J^2 dt, \qquad (4)$$

where L_1 is the inductance-per-unit-length, mainly a geometry parameter. This equation does not include any losses associated with the dynamic efficiency. The impulse bit would be reduced by a factor of one-half, for example, if there was a uniform propellant distribution in the discharge chamber before the pulse [12]. A graph showing measured impulse bit as a function of the measured integral of the current squared is shown in Fig. 12. This graph also contains two lines which show what Eq. 4 predicts using both a slug-like propellant distribution where all the propellant mass is included in the beginning of the discharge and a uniform propellant distribution where the impulse is reduced by half. This graph shows that most of the data follows a linear relation between the impulse bit and the integral of the current squared while falling somewhere between a dynamic efficiency of 50 and 75%.

By considering the relations between the current magnitude and driving capacitance as well as the changing inductance based on the current sheet velocity, two other relations can be derived[2, 5, 11],

$$I_{bit} \propto E L_1 \sqrt{\frac{C}{< L >}}, \qquad (5)$$

$$\eta \propto I_{sp} L_1 \sqrt{\frac{C}{< L >}}, \qquad (6)$$

where $< L >$ is the average inductance as the current sheet propagates down the electrodes. In ref. [5] this term has been replaced by the product of the inductance-per-unit-length times some average length of electrode required to accelerate the current sheet to its final velocity, yielding

$$I_{bit} \propto E \sqrt{\frac{C L_1}{< l_{elec} >}}. \qquad (7)$$

As the electrode geometry does not change throughout the experiment, the terms relating to the inductance should be fairly constant and we should see more of a dependence on thruster performance with the square-root of the capacitance. To demonstrate this trend in the database, a "normalized" impulse bit will be defined as,

$$I_{norm} \equiv \frac{I_{bit}}{E} \sqrt{\frac{< l_{elec} >}{C L_1}}, \qquad (8)$$

with l_{elec} set to a constant value of 8 cm for PT5. A plot showing the normalized impulse with varying mass bit is presented in Fig. 13. This plot, in comparison to Fig. 11(a) shows that, especially for low mass bits (high I_{sp}), the normalized impulse relation collapses all the curves with varying energy and capacitance onto one. In general the trend of the impulse bit scaling with the energy level and square-root of the capacitance level is present throughout the data. The normalized impulse values greater than unity correspond to mass bits > 0.5 μg and Mode I operation as described previously. These higher than expected values could be explained by the choice of a constant $< l_{elec} >$ being the full extent of the electrodes. It could be that at these higher mass bits the current sheet does not travel the complete length before the discharge is extinguished and the normalized impulse should be reduced. This also has implications for

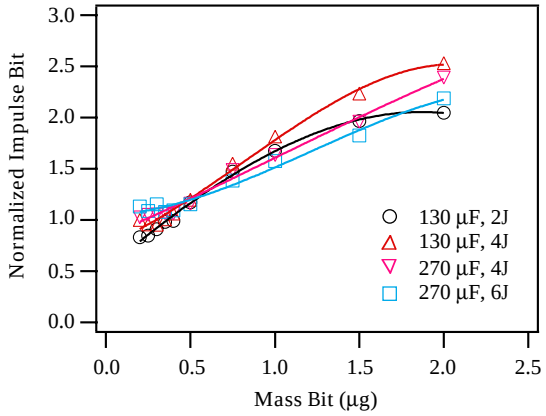

Figure 13: PT5 normalized impulse bit (see Eq. 8) as a function of mass bit at various capacitance and energy levels. The error bars are not larger than the markers.

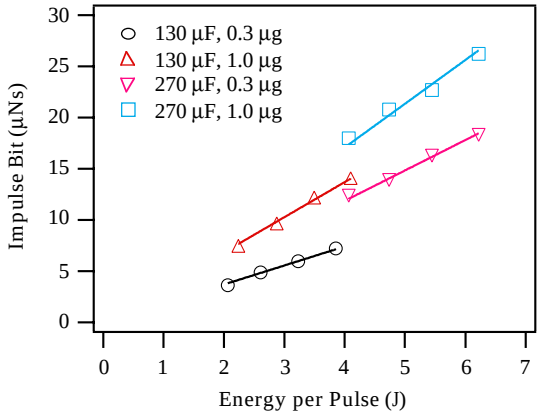

Figure 14: PT5 impulse bit as a function of initial stored discharge energy for two different mass bits and two levels of capacitance.

changing the dynamic efficiency if the mass accumulation process is different is this mode of operation.

Equation 7 implies that the thrust-to-power ratio is dependent on the square-root of the capacitance and is independent on the energy in the pulse. This trend is present in the data as shown in Fig. 14 where the mass bit is held constant and the energy is varied as a parameter in measuring the impulse. The graph shows that the impulse bit is linearly related to the discharge energy for both small and large mass bit values (both Mode I and Mode II operation) and various levels of capacitance. This implies that the thrust-to-power ratio (impulse bit to energy ratio) does not depend on discharge energy which is to be expected in an electromagnetic accelerator.

The dependencies suggested for a thruster where electrothermal acceleration is dominant are quite different[11]. In that case, the impulse bit is expected to scale with the square root of the discharge energy to mass bit ratio and not depend directly on capacitance or inductance change. In addition, the efficiency of a pure electrothermal accelerator is expected to be constant over wide range of specific impulse, energy and mass bit values. While the efficiency as seen in panels c and d of Fig. 11 is indeed independent of mass bit and I_{sp} at high mass bit values (i.e. Mode I), it does show a dependence on energy, albeit a weaker one than for Mode II. This tends to indicate that the acceleration in Mode I may be due to a combination of both electrothermal and electromagnetic effects. Again, as the losses associated with sweeping up the propellant are not accounted for in our predictions, an explanation for trends in Mode I could be a function of improved dynamic efficiency as well.

5.2 Influence of Erosion Products on Performance

Erosion rate measurements conducted at JPL using a slightly smaller, parallel-plate geometry GFPPT have shown that the electrodes, specifically the cathode and spark plug, can erode a significant amount per discharge relatively independent of discharge energy and mass bit levels. It is believed that most of the erosion comes from the stainless-steel spark plug cathode possibly late in the discharge as seen from bright spots near the spark-plugs in Imacon FFT pictures. Currently work is continuing at EPPDyL to quantify the erosion rates of the spark plug ignitors in the coaxial geometry GFPPT. The erosion of electrode material plays, as yet, an unknown role in GFPPT performance. Although preliminary results from measurements at EPPDyL suggest that erosion rates in PT5 are very similar to those measured at JPL, a similarly large amount of material was found to be *added* to the anode PT5 suggesting that the erosion products do not entirely contribute to the exhaust. Experiments are planned at EPPDyL to accurately quantify erosion and deposition rates and asses their influence on performance.

6 Conclusions

The following summary and conclusions can be drawn from the above study:

- Impulse bit measurements with mass bits on the order of 1 μg/s and lower may be affected significantly by contamination from diffusion pumps and required a major renovation of the facilities at EPPDyL including the implementation of LN_2-cooled baffles and the development of a protocol for thruster decontamination which was verified by comparing the data with measurements taken in a cryo-pumped facility.
- A new discharge initiation circuit was required to provide a reliable, symmetric breakdown to begin each pulse, significantly improving thruster performance and shot-to-shot repeatablity.
- With an effective method for measuring the impulse and a repeatable discharge, an argon propellant database was collected over various mass bits, energy levels, and capacitance values.
- Two modes of performance scaling were clearly discerned in each of the performance curves. For all operation parameters fixed, decreasing the mass bit lead to a transition to a mode in which the measured performance scales as theoretically expected from electromagnetic acceleration. Specifically, the impulse bit, efficiency, and thrust-to-power ratio all scale with the square-root of capacitance.

7 APPENDIX: Test Facility Changes

In order to reduce the diffusion pump oil backstreaming rate into the test facility at EPPDyL two major steps were taken: vacuum chamber cleaning and repair as well as the installation of liquid nitrogen cooling lines to the existing baffle system. Both of these renovations will be described in more detail in this section of the paper.

7.1 Vacuum Chamber Cleaning and Repair

The vacuum vessel used for this study is a 2 m diameter, 5 m long fiberglass tank shown in Fig. 15 which is backed by two 48 inch diffusion pumps and a large 1340 cfm roughing system. This facility has accumulated over 50,000 hours of operation since it was first evacuated twenty years ago. Experiments performed in this facility have included use of quasi-steady magnetoplasmadynamic thrusters (MPDTs), ablative pulsed plasma thrusters (APPTs), and many other devices. Over time, residual roughing and diffusion pump oil as well as various erosion products from different experiments have built up on the facility walls. As part of the facility renovations, the entire interior surface of the tank was cleaned by scrubbing with iso-propyl alcohol effectively eliminating the background contaminants from the walls.

The facility has also experienced some surface fatigue due to pressure cycling. This is apparent from the visual cracks in the gel-coat surface covering the fiberglass flanges and optical ports. The cracks produced numerous small leaks which increased the background pressure and, therefore, oil back-streaming rate. The cracks were repaired through a process of grinding out the material around each crack and replacing removed with three layers of gel-coat epoxy. Care was taken to replace the smooth finish of the flange surfaces keeping leaks to a minimum. After all repairs were complete, the facility background pressure was reduced by 50% to an operating pressure now normally below 4×10^{-5} Torr.

7.2 Activation of Liquid Nitrogen Cooled Baffles

Further reduction of diffusion pump oil backstreaming and contamination requires active cooling of baffles or traps very near the diffusion pump entry into the facility. The baffles in the fiberglass facility at EPPDyL (shown in Fig. 15) have been in place since its construction, however, they have not been actively cooled until recently. The baffles used here are low-profile fiberglass cones with a copper plate attached on the underside towards the diffusion pump. Copper tubing (3/8" diameter) is attached to the copper plate with small clamps in a spiral configuration. Only two inches separate each turn of the coil, and the total length of the lines close is to 150 ft. for each baffle. Originally designed for a freon-based cooling system, the baffles have been converted for liquid nitrogen cooling by the installation of new cryo-genic feed-throughs and the replacement of all Swagelok fittings with hard-soldered connections. The baffles are connected in parallel for even cooling and have Type T thermocouples mounted to the inlets and outlets of both baffles inside the tank. Liquid nitrogen is supplied for eight hours at a time by a 160 liter portable

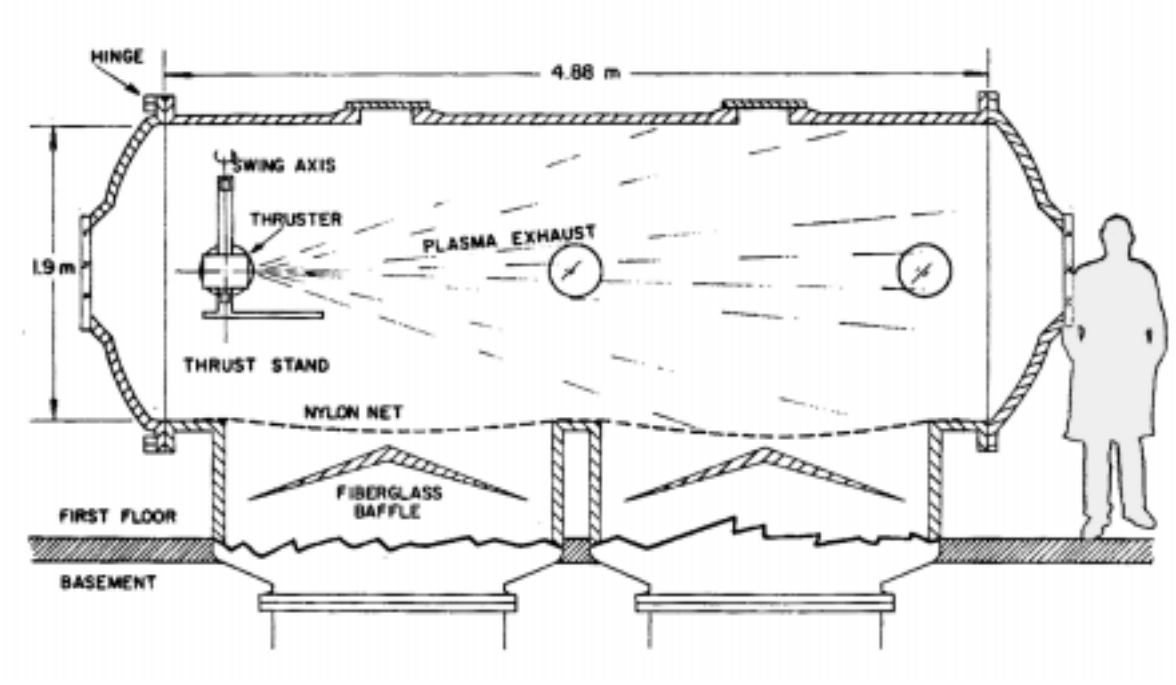

Figure 15: Drawing of the Pulsed Performance Measurement facility at EPPDyL showing thrust stand and baffle location.

dewar that is refilled before each test. Between tests, the baffles are *not* actively cooled requiring a cleaning process before testing as described in Section 3.2.

Slightly more than an hour after activation, the baffles reach their lowest operating temperature of at most $-70°$C as measured by the outlet temperature of the baffle cooling lines. The inlet temperature reaches $-180°$C almost immediately after activation and both baffles generally cool down at the same rate. The background tank pressure typically decreases by 10% due in a large part to the freezing of water vapor to the baffle surface. The baffle operation and cooling rate are very similar from test to test although the outlet temperature of the baffle is verified to be below $-60°$C before any testing begins.

References

[1] J.K. Ziemer and E.Y. Choueiri. Dimensionless performance model for gas-fed pulsed plasma thrusters. In 34^{th} *Joint Propulsion Conference*, Cleveland, Ohio, July 13-15 1998. AIAA 98-3661.

[2] D. Keefer and R. Rhodes. Electromagnetic acceleration in pulsed plasma thrusters. In 25^{th} *International Electric Propulsion Conference*, Cleveland, Ohio, August 24-28 1997. IEPC 97-035.

[3] P.G. Mikellides, P.J. Turchi, et al. Theoretical studies of a pulsed plasma microthruster. In 25^{th} *International Electric Propulsion Conference*, Cleveland, Ohio, August 24-28 1997. IEPC 97-037.

[4] J.K. Ziemer, E.A. Cubbin, E.Y. Choueiri, and D. Birx. Performance characterization of a high efficiency gas-fed pulsed plasma thruster. In 33^{rd} *Joint Propulsion Conference*, Seattle, Washington, July 6-9 1997. AIAA 97-2925.

[5] J.K. Ziemer, E.Y. Choueiri, and D. Birx. Trends in performance improvements of a gas-fed pulsed plasma thruster. In 25^{th} *International Electric Propulsion Conference*, Cleveland, Ohio, August 24-28 1997. IEPC 97-040.

[6] W.J. Guman and W. Truglio. Surface effects in a pulsed plasma accelerator. *AIAA Journal*, 2(7):1342–1343, July 1964.

m_{bit} (μg)	I_{bit} (μN-s)	I_{sp} (s)	η (%)
0.20	11.6	5940	8.53
0.25	12.0	4890	7.20
0.30	11.9	4060	6.01
0.35	12.0	3500	5.22
0.40	12.0	3060	4.56
0.50	13.2	2680	4.35
0.75	16.9	2290	4.77
1.00	18.6	1900	4.35
1.50	22.3	1520	4.16
2.00	27.6	1410	4.70

Table 1: PT5 performance data for a fixed energy of 4.0±0.1 J and a capacitance value of 270±3 μF. The last row in the table is the average error from each measurement.

m_{bit} (μg)	I_{bit} (μN-s)	I_{sp} (s)	η (%)
0.20	19.5	9930	15.8
0.25	18.6	7600	11.6
0.30	19.8	6720	10.9
0.35	18.5	5400	8.16
0.40	18.6	4740	7.26
0.50	19.5	3990	6.42
0.75	23.2	3160	6.12
1.00	26.3	2680	5.91
1.50	31.1	2120	5.40
2.00	37.1	1890	5.79

Table 2: PT5 performance data for a fixed energy of 6.0±0.1 J and a capacitance value of 270±3 μF. The last row in the table is the average error from each measurement.

[7] J.K. Ziemer, T.E. Markusic, E.Y. Choueiri, and D. Birx. Effects of ignition on discharge symmetry in gas-fed pulsed plasma thrusters. In 34^{th} *Joint Propulsion Conference*, Cleveland, Ohio, July 13-15 1998. AIAA 98-3803.

[8] M.E. Brady and G. Aston. Pulsed plasma thruster ignitor plug ignition characteristics. *Journal of Spacecraft and Rockets*, 20(5):450–451, 1983.

[9] E.A. Cubbin, J.K. Ziemer, E.Y. Choueiri, and R.G. Jahn. Laser interferometric measurements of impulsive thrust. *Review of Scientific Instruments*, 68(6):2339–2346, 1997.

[10] T.W. Haag. PPT thrust stand. In 31^{st} *Joint Propulsion Conference*, San Diego, California, July 1995. AIAA 95-2917.

[11] W.J. Guman. Solid propellant pulsed plasma micro-thruster studies. In 6^{th} *Aerospace Sciences Meeting*, New York, New York, January 22-24 1968. AIAA 68-85.

[12] N.A. Black and R.G. Jahn. Dynamic efficiency of pulsed plasma accelerators. *AIAA Journal*, 3(6):1209–1210, June 1965.

m_{bit} (μg)	I_{bit} (μN-s)	I_{sp} (s)	η (%)
0.20	3.32	1690	1.37
0.25	3.39	1380	1.15
0.30	3.64	1240	1.10
0.35	3.97	1160	1.11
0.40	4.00	1020	0.99
0.50	4.80	980	1.12
0.75	6.24	848	1.21
1.00	7.42	757	1.23
1.50	9.30	632	1.21
2.00	9.75	497	0.99
±2%	±8%	±5%	±10%

m_{bit} (μg)	I_{bit} (μN-s)	I_{sp} (s)	η (%)
0.20	7.68	3920	3.81
0.25	7.38	3010	2.80
0.30	7.32	2490	2.31
0.35	7.74	2260	2.21
0.40	8.21	2090	2.16
0.50	9.29	1900	2.20
0.75	12.2	1670	2.50
1.00	14.7	1500	2.64
1.50	18.7	1270	2.76
2.00	21.4	1091	2.68
±2%	±8%	±5%	±10%

Table 3: PT5 performance data for a fixed capacitance value of 130±2 μF and energy levels of 2.1±0.1 J and 4.0±0.1 J. The last row in the table is the average error from each measurement.